



UNIVERSIDADE ESTADUAL DE CAMPINAS
SISTEMA DE BIBLIOTECAS DA UNICAMP
REPOSITÓRIO DA PRODUÇÃO CIENTÍFICA E INTELLECTUAL DA UNICAMP



Versão do arquivo anexado / Version of attached file:

Versão do Editor / Published Version

Mais informações no site da editora / Further information on publisher's website:

<https://www.nature.com/articles/srep06543>

DOI: 10.1038/srep06543

Direitos autorais / Publisher's copyright statement:

©2014 by Nature Publishing Group. All rights reserved.

DIRETORIA DE TRATAMENTO DA INFORMAÇÃO
Cidade Universitária Zeferino Vaz Barão Geraldo
CEP 13083-970 – Campinas SP
Fone: (19) 3521-6493
<http://www.repositorio.unicamp.br>



OPEN

SUBJECT AREAS:

METALS AND ALLOYS

SUPERCONDUCTING PROPERTIES
AND MATERIALS

Received

12 March 2014

Accepted

15 September 2014

Published

8 October 2014

Correspondence and
requests for materials
should be addressed to
P.F.S.R. (pfsrosa@uci.
edu)

Site specific spin dynamics in BaFe_2As_2 : tuning the ground state by orbital differentiation

P. F. S. Rosa^{1,2}, C. Adriano¹, T. M. Garitezi¹, T. Grant², Z. Fisk², R. R. Urbano¹ & P. G. Pagliuso¹

¹Instituto de Física “Gleb Wataghin”, UNICAMP, Campinas-SP, 13083-859, Brazil, ²University of California, Irvine, California 92697-4574, USA.

The role of orbital differentiation on the emergence of superconductivity in the Fe-based superconductors remains an open question to the scientific community. In this investigation, we employ a suitable microscopic spin probe technique, namely Electron Spin Resonance (ESR), to investigate this issue on selected chemically substituted BaFe_2As_2 single crystals. As the spin-density wave (SDW) phase is suppressed, we observe a clear increase of the Fe 3d bands anisotropy along with their localization at the FeAs plane. Such an increase of the planar orbital content is interestingly independent of the chemical substitution responsible for suppressing the SDW phase. As a consequence, the magnetic fluctuations in combination with this particular symmetry of the Fe 3d bands are propitious ingredients for the emergence of superconductivity in this class of materials.

The structural parameters in low-symmetry layered systems, such as the iron pnictides/chalcogenides, cuprates and the heavy fermion (HF) compounds have played an important role in determining both symmetry and dimensionality of the magnetic fluctuations^{1–3}. An immediate consequence of a structural control (or tuning) parameter is its influence on the crystalline electrical field (CEF) effects, which are often relevant in determining the ground state in strongly correlated materials. Particularly for the HF superconductors, the *f*-electrons strongly hybridize with conduction electron (*ce*) bands and the single-ion anisotropy, mostly defined by the CEF effects, influences the magnetic fluctuations at the Fermi surface (FS)^{4–8}. In fact, the superconducting transition temperature (T_c) scales with the lattice parameter ratio *c/a* for several HF systems^{4,8}. Yet for the high- T_c cuprates, some structural parameters, such as the Cu-apical oxygen distance and the bond length between Cu and the in-plane oxygen, have been suggested as control parameters of T_c . Remarkably, the apical oxygen distance to the CuO_2 plane also displays a reasonable scaling with T_c ^{9,10}. In the same fashion, the Fe-pnictide distance has been recently suggested as a similar control parameter tuning the CEF levels in the Fe-based compounds and, consequently, changing the orbital contributions to the bands at the Fermi level^{11,12}. Moreover, it is notorious that this orbital interplay is indeed crucial to the formation of the spin-density wave (SDW) phase due to the \mathbb{Z}^2 symmetry break (or *xz/yz* orbitals). Nonetheless, the ultimate role of the orbital degrees of freedom on the emergence of superconductivity in Fe-pnictides materials remains an unsolved puzzle.

In this regard, several spin probes such as electron spin resonance (ESR), nuclear magnetic resonance (NMR), muon spin rotation (μSR), Mössbauer spectroscopy, and magnetic neutron scattering, can in principle be used to explore the CEF and orbital differentiation effects on the spin dynamics of a system and their possible influence over its superconducting order parameter. The observation of homogeneous resonances by such techniques in strongly correlated metals allows one to obtain the imaginary part of the spin susceptibility $\chi''(\mathbf{q}, \omega)$. In particular, the ESR absorption line of a paramagnetic local probe is a measure of $\chi''(\mathbf{q}, \omega)$, which in turn is directly related to the spin-lattice relaxation rate ($1/T_1$) of the localized resonating spins through the *ce* and thus to the lattice^{13,14}. In a general approach for dilute local moments in metals, the ESR linewidth is linear in temperature and can be written as $\Delta H = a + bT$, the so-called Korringa relaxation¹⁵. The residual linewidth, *a*, arises from the spin-spin interactions of local moments, lattice defects, *g*-factor distribution, and perhaps unresolved hyperfine and crystalline electrical field (CEF) fine structures. In addition, the thermal broadening *b* is defined as:

$$b \equiv \frac{d(\Delta H)}{dT} = \frac{\pi k_B}{g\mu_B} \langle J_f^2(\mathbf{q}) \rangle \eta^2(E_F) \frac{K(\alpha)}{(1-\alpha)^2}. \quad (1)$$



Here, $\langle J_{fs}(\mathbf{q}) \rangle^{1/2}$ is the effective exchange interaction between the local moment and the *ce* in the presence of *ce* momentum transfer averaged over the whole FS¹⁶, $\eta(E_F)$ is the “bare” density of states (DOS) for one spin direction at the Fermi level, k_B is the Boltzmann constant, μ_B is the Bohr magneton, g is the local moment *g*-value and $K(\alpha)$ is the Korringa exchange enhancement factor due to electron-electron exchange interaction^{19,20}. Here “bottleneck”, “dynamic” effects, and multiple bands effects are not present²¹. These are reasonable assumptions because when “dynamic” effects are present the *g*-values are usually strongly *T*-dependent and when the bottleneck effect is relevant the Korringa rate *b* decreases with an increasing concentration of the magnetic ions²¹. Concerning the case of multiple band effects, one would expect the calculated *g*-shift to be much smaller than the measured one^{22–24}. As an example, we consider the pure EuFe₂As₂ compound in the simplest scenario for the treatment of exchange interaction between Eu²⁺ spins and conduction electron spins, i.e., $b = (\pi k_B / g \mu_B) \Delta g$. By replacing Δg by its experimental value $\Delta g \sim 0.05$ one gets a Korringa rate of $b \sim 150$ Oe/K, which is much larger than the measured one. This result is not only valid for the pure compound but also for the samples studied in the present work, which present the same *g*-shift. Thus, none of the above mentioned effects have been observed in the studied temperature range in previous works²⁶, nor in our present ESR data. In fact, a smaller experimental Korringa rate implies that one needs to take into account *q*-dependent exchange interaction and perhaps conduction electron-electron correlations as the dominant effects, which were already included in Eq. (1) of the present manuscript. The *g*-shift Δg can thus be written as²⁵:

$$\Delta g \equiv g - g_{insulator} = J_{fs}(\mathbf{0}) \frac{\eta(E_F)}{1 - \alpha}. \quad (2)$$

At the local moment site, the *g*-shift probes the *ce* polarization ($\mathbf{q} = 0$). On the other hand, the Korringa rate probes the *ce* momentum transfer ($0 \leq \mathbf{q} \leq 2k_F$) averaged over the FS¹⁶. Thus, from Eqs. 1 and 2 one obtains information about the density of states at the Fermi level as well as the strength and *q*-dependence of the exchange interaction.

Previous studies on the series Ba_{1-x}Eu_xFe₂As₂ have shown that $\langle J_{fs}^2(\mathbf{q}) \rangle^{1/2}$ decreases with decreasing Eu content²⁶. The scaling of $\langle J_{fs}^2(\mathbf{q}) \rangle^{1/2}$ with T_{SDW} suggests that the electron bands with appreciable overlap with the Eu²⁺ 4*f* states become more anisotropic (less *s*-like) as the SDW phase is suppressed. Moreover, these electron bands also move, on average, further away from the Eu²⁺ sites in real space²⁶. Therefore, in order to generalize such a scenario and further investigate the role of symmetry changes in highly occupied 3*d* bands in superconducting members of this family, we perform in the present report a systematic ESR study on Ba_{1-x}Eu_xFe_{2-y}M_yAs₂ single crystals (with *M* standing for transition metals Co, Cu, Mn, Ni, and Ru). It is worth pointing out that the Ba and FeAs planes are probed by the ESR active Eu²⁺ and Mn²⁺/Cu²⁺ paramagnetic spins, respectively. The ($x = 0.2$; $y = 0$) compound was taken as reference for the evolution of the spin dynamics as a function of *M* substitution (*y* content) because it is the lowest Eu concentration presenting Korringa relaxation.

Starting off with the macroscopic physical properties, Fig. 1a displays the temperature dependence of the normalized electrical resistivity for the studied single crystals. Room-*T* values of $\rho(T)$ vary within the range 0.2–0.8 mΩ.cm. Except for *M* = Ru, which displays the smallest substitution content ($y = 0.01$), the electrical resistivity increases at T_{SDW} , as typically found for doped BaFe₂As₂ samples²⁷. Besides, for the chosen reference compound ($x = 0.2$; $y = 0$), a metallic behaviour is observed down to T_{SDW} where a sudden drop at 137 K is identified in its dataset. A suppression of the SDW phase with lower transition temperatures of 135 K, 102 K, 98 K, and 86 K is clearly observed as Fe is replaced by transition metals *M* = Ru, Ni,

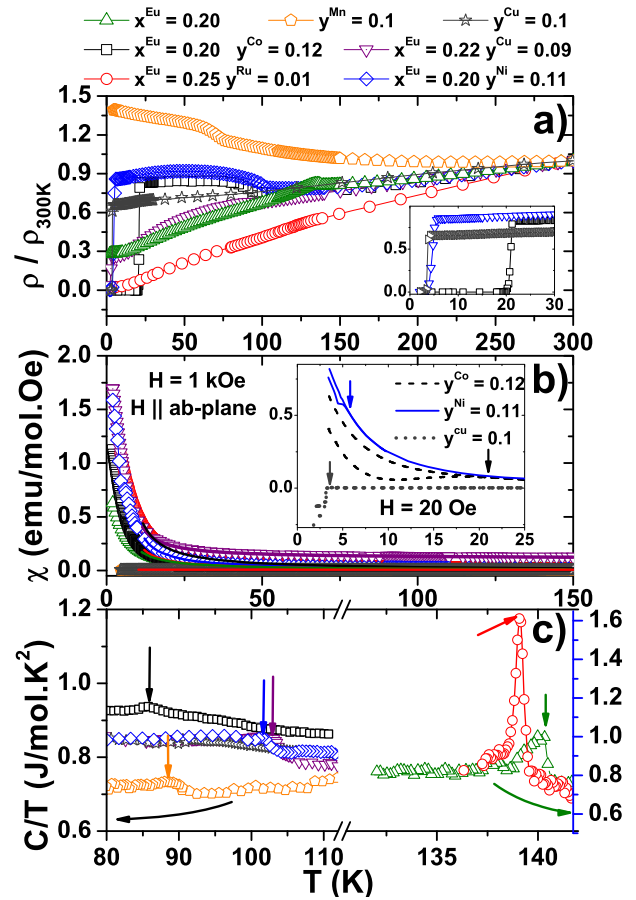


Figure 1 | Thermodynamic properties of the Ba_{1-x}Eu_xFe_{2-y}M_yAs₂ single crystals. The insets show a) the zero electrical resistivity at the superconducting transition and, b) zero-field cooling/field cooling magnetic susceptibilities.

Cu, and Co, respectively. Superconductivity also emerges for Co and Ni substitutions with $T_c = 22$ K and 6 K, respectively (inset to Fig. 1a). In good agreement, the SDW phase is also suppressed for BaFe_{2-y}M_yAs₂ (i.e., $x = 0$) in comparison with the parent BaFe₂As₂ with $T_{SDW} \simeq 140$ K. This can be noted for the $y_{Mn} = 0.1$ compound with $T_{SDW} = 78$ K. In particular, the SDW phase is fully suppressed for $y_{Cu} = 0.1$ giving way to superconductivity at $T_c = 3.8$ K (inset to Fig. 1a).

Fig. 1b shows the in plane magnetic susceptibility as a function of temperature for $H = 1$ kOe. For all samples, $\chi(T)$ is well fit to the Curie-Weiss law plus a *T*-independent Pauli term, $\chi(T) = \chi_0 + C/(T - \theta_{CW})$ (solid lines). We obtain an effective moment $\mu_{eff} \approx 8\mu_B$ from the Eu²⁺ ions and an electronic spin susceptibility of $\chi_0 = 2(1) \times 10^{-3}$ emu/mol-Oe for all compounds. The superconducting transition at low-field ($H = 20$ Oe) is defined by the arrows in the inset of Fig. 1b. It is worth noting that, for *M* = Co and Ni, the diamagnetic response below T_c is overcome by the Eu²⁺ paramagnetic one. Fig. 1c shows the *T*-dependence of the specific heat for the selected single crystals. For the reference compound with $x = 0.2$ and $y = 0$, the SDW transition is defined by a jump at 137 K (green arrow). In agreement with the ρ data of Figs. 1a–1b, we observed a suppression of the SDW phase as Fe is substituted by transition metals *M*.

Now we turn our attention to the ESR results on the selected single crystals in the paramagnetic (PM) state ($T > T_{SDW}$). A single asymmetric Dysonian ESR resonance is observed for all compounds, meaning that the skin depth is smaller than the sample dimensions²⁸. Nonetheless, as presented in Fig. 2, the X-Band ($\nu \simeq 9.5$ GHz) ESR spectra at room-*T* become Lorentzian-like after gently crushing the single crystals in order to improve the signal to noise ratio. From fits

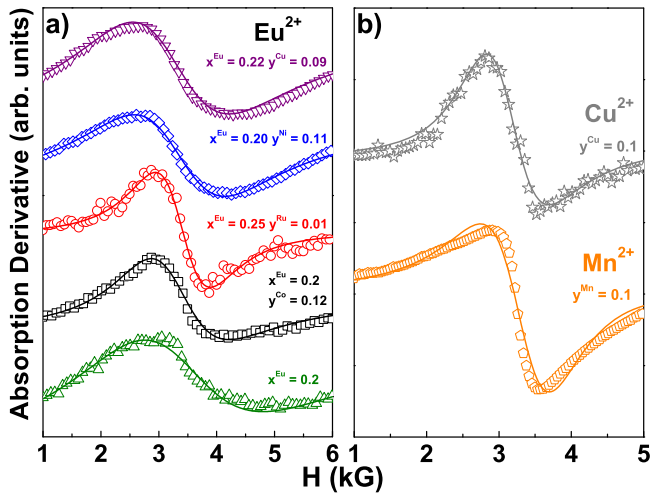


Figure 2 | X-Band (~ 9.5 GHz) ESR spectra of $\text{Ba}_{1-x}\text{Eu}_x\text{Fe}_{2-y}\text{M}_y\text{As}_2$ single crystals at room temperature.

to the resonances using the appropriate admixture of absorption and dispersion (solid lines), we obtained the T -dependence of both the linewidth ΔH and g -values presented in Fig. 3.

A linear (Korringa) increase of ΔH with increasing- T is observed for the Eu^{2+} ESR signal in the PM state, as shown in Fig. 3a. From linear fits to $\Delta H(T)$ above T_{SDW} we extracted the values of the Korringa rate $b \equiv \Delta H/\Delta T$. It is evident that b decreases systematically for any of the transition metal substitution. On the other hand, Fig. 3b shows that, when $x = 0$ and $M = \text{Mn}^{2+}$ or Cu^{2+} , the ESR signal from these magnetic probes broadens as the temperature is lowered indicating that a competition between the spin-spin and spin- ce interactions must be occurring. However, in the high- T range, the Korringa-like relaxation dominates for the $y=0.1$ samples. We will discuss the behavior of the dilute samples ($y=0.01$) below. Thus, linear fits to $\Delta H(T)$ allowed us to obtain $b_{\text{Mn}^{2+}} = 1.1(2)$ Oe/K and $b_{\text{Cu}^{2+}} = 3.5(2)$ Oe/K, respectively.

The T -dependence of the Eu^{2+} ESR g -value in the normal state is presented in Fig. 3c. Before the long range SDW order sets in, a roughly T -independent $g \approx 2$ is commonly observed for the Eu^{2+} ESR signal, as previously suggested by reports on EuFe_2As_2 , $\text{Eu}_{0.5}\text{K}_{0.5}\text{Fe}_2\text{As}_2$ and $\text{EuFe}_{2-x}\text{Co}_x\text{As}_2$ ^{32–34}. In fact, the high- T Eu^{2+} g -values of our $\text{Ba}_{1-x}\text{Eu}_x\text{Fe}_{2-y}\text{M}_y\text{As}_2$ single crystals are, on average, equal to $2.04(4)$ and independent of the Eu^{2+} content x . For the narrowest ESR linewidths, we are able to determine the g -value with higher precision, $g = 2.05(3)$. As it can be verified in Fig. 3c, such a value is indeed a reasonable mean g -value for all x with $T > T_{\text{SDW}}$.

Based on the framework discussed in Ref. 26, we now show that possible changes in the DOS as well as any evolution of the electron-electron interaction cannot account for the Korringa suppression observed as a function of M substitution. In order to evaluate the possible contribution of e-e correlations in our ESR data, we note that the electronic spin susceptibility obtained experimentally is $\chi_0 = 2(1) \times 10^{-3}$ emu/mol-Oe for all studied compounds. This value is about one order of magnitude larger than the magnetic Pauli susceptibility estimated from the heat capacity coefficient γ , indicating that an e-e exchange enhancement contributes to the ce spin susceptibility in the series. Thus, in the presence of such an enhancement, the host metal ce spin susceptibility can be approximated by:

$$\chi_0 = 2 \mu_B^2 \frac{\eta(E_F)}{1 - \alpha}, \quad (3)$$

where α accounts for the e-e interaction, $(1 - \alpha)^{-1}$ is the Stoner enhancement factor and $\eta(E_F)$ is the “bare” DOS for one spin direction at E_F ^{30,31}. Now, assuming that the enhancement in χ_0 is only due to e-e interaction, an $\alpha \approx 0.85(5)$ can be estimated.

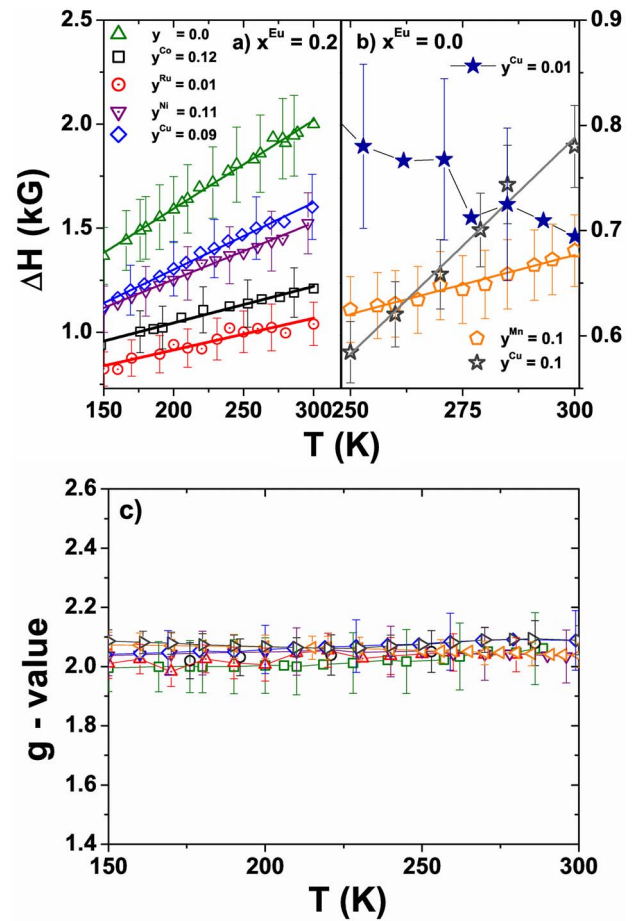


Figure 3 | T -dependence of a-b) the ESR linewidth ΔH and c) the g -values measured for $\text{Ba}_{1-x}\text{Eu}_x\text{Fe}_{2-y}\text{M}_y\text{As}_2$ compounds.

Consequently, based on Ref. 20 one can determine the corresponding $K(\alpha) = 0.2(1)$. Then, using the relation $(\pi k_B/g\mu_B) = 2.34 \times 10^4$ Oe/K and replacing $\Delta g \approx 0.05(3)$, $\eta(E_F) = 3.34$ states/eV mol-spin and b values from Table 1 into Eqs. 1 and 2, we were able to extract $J_{fs}(0) = 2(1)$ meV and $\langle J_{fs}^2(\mathbf{q}) \rangle^{1/2}$ for all compounds. These values are also presented in Table 1.

Based on the data of Figs. 1–3, the diagrams shown in Fig. 4 summarize the behaviour of T_{SDW} and Korringa relaxation rate b against M substitution. When the ESR spin probe is out of the Fe-As plane (Fig. 4a), we observe that both T_{SDW} and b values are suppressed with respect to their values for $\text{Ba}_{0.8}\text{Eu}_{0.2}\text{Fe}_2\text{As}_2$ as Fe is substituted by M . Nevertheless, when the spin probe is in-plane (Fig. 4b), the opposite behaviour takes place and the Korringa rate b increases as the SDW phase is suppressed. Interestingly, for smaller Mn and Cu concentrations of the order of $\sim 0.5\%$, the ESR linewidth broadens with decreasing temperature in the entire temperature range. In particular, Fig. 3b includes the thermal broadening for the $y^{\text{Cu}} = 0.01$ sample. In this case, the Korringa rate, if it exists, would be at least smaller than the thermal broadening observed, otherwise it would be detectable. Thus, one can infer that the Korringa rate for the Cu sample is indeed decreasing for smaller concentrations. On the other hand, it is not straightforward to infer such conclusion from ESR data on lower concentrations of Mn since the Korringa rate for higher concentrations is already very small (~ 1 Oe/K). Nevertheless, for both in-plane probes, the Korringa behavior is overcome by the spin-spin interactions associated with the proximity to a magnetic SDW phase. Furthermore, it is worth noting that $3d$ ions in low symmetry metallic hosts are most likely to display quench of the angular momentum and thus spin-only wave



Table 1 | Experimental ESR Korringa rate b , the g -values, the g -shift Δg , the exchange interaction $J_{fs}(0)$ and calculated $\langle J_{fs}^2(\mathbf{q}) \rangle^{1/2}$ for all samples studied in this work. As defined in Eq. 2, $\Delta g \equiv g - g_{insulator}$. For Eu^{2+} , $g_{insulator}$ is well known to be $1.993(1)^{13}$. For Mn^{2+} , an average of g value in similar insulating compounds leads to $2.00(5)^{13}$. For Cu^{2+} , we assume that the magnetic moment is entirely due to the spin and the $g_{insulator} \sim 2$. Although this assumption leads to a significant error in $J_{fs}(0)$, it does not affect the Korringa-like analysis (Eq. 1)^{16–18}

Sample	b (Oe/K)	g -value	Δg	$J_{fs}(0)$ meV	$\langle J_{fs}^2(\mathbf{q}) \rangle^{1/2}$ (meV)
$\text{Ba}_{0.8}\text{Eu}_{0.2}\text{Fe}_2\text{As}_2$ (ref. compound)	4.3(2)	2.04(4)	0.05(3)	2(1)	1.4(8)
$\text{BaFe}_{1.9}\text{Cu}_{0.1}\text{As}_2$	3.5(2)	2.08(4)	0.08(3)	2(1)	1.2(6)
$\text{Ba}_{0.78}\text{Eu}_{0.22}\text{Fe}_{1.91}\text{Cu}_{0.09}\text{As}_2$	2.8(2)	2.05(4)	0.06(4)	2(1)	1.1(8)
$\text{Ba}_{0.8}\text{Eu}_{0.2}\text{Fe}_{1.89}\text{Ni}_{0.11}\text{As}_2$	2.5(2)	2.04(4)	0.05(3)	2(1)	1.0(8)
$\text{Ba}_{0.8}\text{Eu}_{0.2}\text{Fe}_{1.88}\text{Co}_{0.12}\text{As}_2$	1.7(2)	2.05(3)	0.06(3)	2(1)	0.9(7)
$\text{Ba}_{0.75}\text{Eu}_{0.25}\text{Fe}_{1.99}\text{Ru}_{0.01}\text{As}_2$	1.5(2)	2.04(3)	0.05(3)	2(1)	0.8(7)
$\text{BaFe}_{1.88}\text{Mn}_{0.12}\text{As}_2$	1.1(2)	2.04(3)	0.05(3)	2(1)	0.7(6)

functions. In fact, our experimental data show that the g -factor is approximately 2 for both Mn and Cu ESR lines. Therefore, it is reasonable to assume that the overlap with the conduction electrons will not differ dramatically between Mn and Cu and in turn their Korringa rates for 5% concentrations could be compared.

Therefore, these results combined evidence that, when the probe is out of (in) the Fe-As plane, the relative value of $\langle J_{fs}^2(\mathbf{q}) \rangle^{1/2}$ clearly decreases (increases) with M -substitution. Given that $J_{fs}(\mathbf{q})$ is the Fourier transform of the spatially varying exchange interaction, by suppressing the SDW phase by M substitution, the electron bands with appreciable overlap with the Eu^{2+} 4f states become more anisotropic (less s -like). Moreover, these bands, on average, move further away from the Eu^{2+} sites in real space, i.e., they assume a more

planar/ xy -orbital character. In fact, in Fig. 4a one can clearly observe a scaling between the magnitude of the SDW phase suppression and that of the Korringa rate, except for the Ru substitution. This is because the particularities in the distortion of the electronic bands may behave differently for each transition metal. For instance, if the chemical substitution is not coherent, interference can occur among the 3d bands and consequently the suppression of the Korringa rate b might be more effective than that of T_{SDW} ²⁹.

It is imperative to notice that our findings are in complete agreement with the data on the concentrated Eu regime. A slower Korringa rate b has also been observed when K or Co were introduced into EuFe_2As_2 ^{33,34}. Furthermore, DFT+DMFT calculations have recently shown that orbital differentiation is crucial when magnetic correlations become relevant in BaFe_2As_2 ¹². By decreasing the iron-pnictogen distances, the xy orbital occupancy increases. This in turn weakens the Fe magnetic moment.

Furthermore, this change in occupancy also affects the Fermi surface since a decrease in the occupancy of the xy orbital results in the increase of the hole pocket size, as seen by ARPES studies in several AFe_2As_2 families^{36,37}. In particular, a comparison between ARPES measurements for BaFe_2As_2 and EuFe_2As_2 in the paramagnetic regime reveals that the xy hole-pocket is twice as large in EuFe_2As_2 , suggesting a decrease of planar xy occupation.

In order to give this reasoning a more graphical view, we have explored how the exchange interaction J between the 3d conduction electrons and the local spin ESR probes may be affected by the orbital differentiation of the 3d bands. As such, we assume a scenario where J is proportional to the overlap between the atomic orbitals. Although simplified, this procedure can qualitatively capture the main features of the orbital differentiation through minute changes in J . Therefore, when the paramagnetic probe is out of the Fe-As plane, one can calculate the squared overlap between Eu 4f and Fe 3d orbital wavefunctions, $\langle \Psi_{4f} | \Psi_{3d} \rangle^2$, as a function of the distance between the Eu and Fe ions, namely z_0 . More specifically, the Fe 3d wave-function is written as $\Psi_{3d} = R_{3d}(x, y, z)[B_{XZY}(\Phi_X z(x, y, z) + \Phi_Y z(x, y, z)) + B_{XY} \Phi_{XY}]$, where $R_{3d}(x, y, z)$ is the 3d radial wave-function and $\Phi(x, y, z)$ are the cubic harmonics for each orbital. Ultimately, as shown in Eq. 1, the crucial result within this scenario is that the Korringa relaxation rate b is directly proportional to $\langle \Psi_{4f} | \Psi_{3d} \rangle^2$.

Let us first consider the overlap between an isotropic Eu 4f configuration and the Fe t_{2g} orbitals: xy and xz/yz . The triplet orbitals were chosen here due to their predominant role on the FS¹². The squared overlap $\langle \Psi_{4f}^{\text{Eu}} | \Psi_{3d}^{\text{Fe}} \rangle^2$ between the Eu 4f and the Fe 3d wavefunctions as a function of z_0 , normalized by the atomic radius of Eu^{2+} ($z_0 = 3.5$ atomic units), is presented in Fig. 5a. We note that, when the planar xy orbital component is the dominant one (solid red line), its squared overlap with the 4f wavefunction decreases slightly faster than that with only xz/yz orbital components (dotted blue lines). One would expect such behaviour simply because the overlap

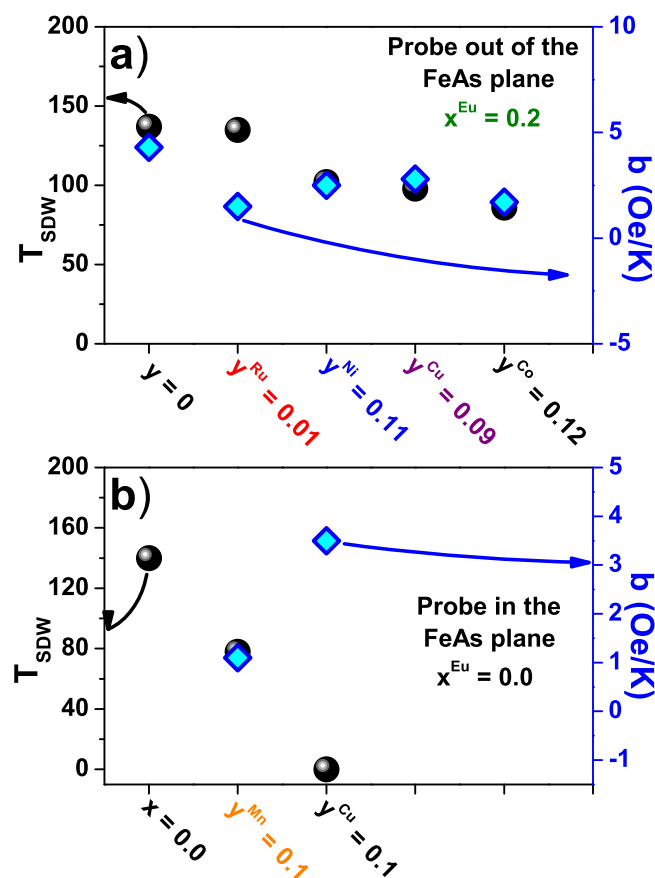


Figure 4 | Spin-density wave transition temperature T_{SDW} and Korringa rate b as a function of transition metal substitution M when the ESR spin probe is a) out of the Fe-As plane and, b) in the Fe-As plane.

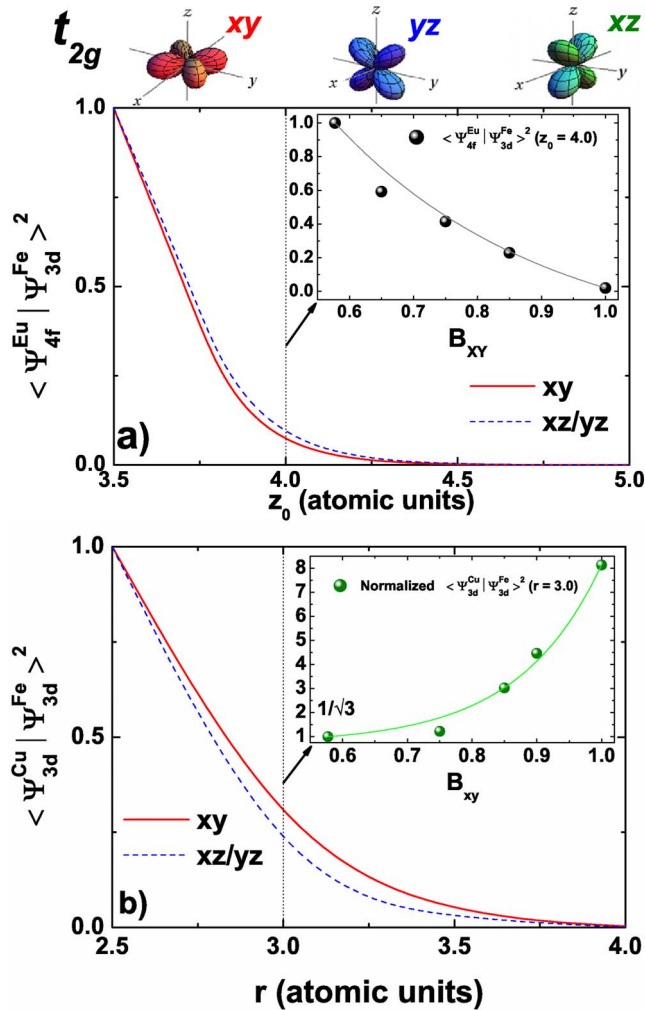


Figure 5 | Squared overlap between the Eu 4f isotropic wavefunction and the t_{2g} Fe 3d wavefunctions xy ($B_{xy} = 1.0$) and xz/yz ($B_{xy} = 0.0$) when a) the probe is at the Fe-As plane; b) the probe is out of the Fe-As plane.

between an 4f isotropic wave function and a 2D wave function decreases faster as the probe moves away from the Fe-As plane when compared to a more 3D wave function with z components.

Moreover, we can now roughly simulate each Fe t_{2g} orbital contribution to the FS using this phenomenological model. Starting with an isotropic Fe 3d configuration, i.e., a normalized population of $1/\sqrt{3}$ for each considered 3d orbital, we are able to tune the xy orbital population - represented by the B_{xy} coefficient - from $1/\sqrt{3}$ up to 1. The inset of Fig. 5a shows $\langle \Psi_{4f}^{Eu} | \Psi_{3d}^{Fe} \rangle^2$ at a particular Eu-Fe distance $z_0 = 4.0$, chosen to better illustrate the behaviour mentioned above. It is clear that, by increasing the xy orbital contribution, the $\langle \Psi_{4f}^{Eu} | \Psi_{3d}^{Fe} \rangle^2$ diminishes drastically, in agreement with the behaviour presented by the Korringa rate b in Fig. 4a for the transition metal M substitution into $\text{Ba}_{0.8}\text{Eu}_{0.2}\text{Fe}_{2-y}\text{M}_y\text{As}_2$.

We now turn our attention to the particular case that considered the local probe in the Fe-As plane ($M = \text{Cu}$). In this case, we are able to calculate $\langle \Psi_{3d}^{Cu} | \Psi_{3d}^{Fe} \rangle^2$ as a function of the radius r from a Fe atom. Fig. 5b displays the calculated squared overlap between the Cu 3d and the Fe 3d wavefunctions with the same t_{2g} orbital configurations of Fig. 5a. However, when the planar xy orbital component is the dominant contribution (solid red line) in this case, the overlap

$\langle \Psi_{3d}^{Cu} | \Psi_{3d}^{Fe} \rangle^2$ decreases slower than that for the xz/yz configuration. The inset of Fig. 5b shows an exponential increase of this squared overlap at $r = 3.0$ atomic units as a function of the xy weight, indicating that higher planar contributions leads to higher Korringa rate b , in good agreement with our experimental data shown in Fig. 4b.

In summary, we have employed a sensitive microscopic spin probe to study the suppression of the SDW magnetic phase in BaFe_2As_2 via transition metal substitution. We demonstrated that the 3d electrons tend to localize at the Fe-As plane as the SDW phase is suppressed due to changes in the structural parameters, independent of the chosen transition metal substitution. When the Fe-As distances are lowered either by chemical substitution or hydrostatic pressure, the crystal field splittings change and, in turn, the planar ($xy/x^2 - y^2$) orbital character of the Fe 3d bands is strongly enhanced at the Fermi level. These effects and consequent orbital differentiation corroborate to the suppression of the itinerant SDW magnetic order and the subsequent emergence of the magnetic-mediated superconductivity in these materials.

This work was supported by FAPESP, AFOSR MURI, CNPq, FINEP-Brazil and NSF-USA.

Methods

Single crystals of $\text{Ba}_{1-x}\text{Eu}_x\text{Fe}_{2-y}\text{M}_y\text{As}_2$ ($M = \text{Mn, Co, Cu, Ru, and Ni}$) were grown using In-flux as described in Ref. 35. The single crystals were checked by X-ray powder diffraction and submitted to elemental analysis using a commercial Energy Dispersive Spectroscopy (EDS) microprobe. No In-incorporation was detected in the crystals. From EDS analysis, we have extracted the actual x_{Eu} and y_{M} concentrations used throughout the text. The in-plane resistivity was measured using a four-probe method. Specific heat data were taken in a commercial small-mass calorimeter and the magnetization data was collected using a superconducting quantum interference device (SQUID) magnetometer. X-Band ($\nu = 9.34$ GHz) ESR measurements were carried out in a commercial Bruker spectrometer with a continuous He gas-flow cryostat.

- Stewart, G. Heavy Fermion Systems. *Rev. Mod. Phys.* **56**, 755787 (1984).
- Monthoux, P. & Lonzarich, G. G. Magnetically mediated superconductivity in quasi-two and three dimensions. *Phys. Rev. B* **63**, 054529 (2011).
- Ong, T. T. & Coleman, P. Local Quantum Criticality of an Iron-Pnictide Tetrahedron. *Phys. Rev. Lett.* **108**, 107201 (2002).
- Pagliuso, P. G. *et al.* Structurally tuned superconductivity in heavy-fermion CeMIn_5 ($M = \text{Co, Ir, Rh}$). *Physica B: Condensed Matter*, Vol. 320, Issues 1–4 2002.
- Pagliuso, P. G. *et al.* Multiple phase transitions in $\text{Ce}(\text{Rh, Ir, Co})\text{In}_5$. *Physica B* **312–313** (2009) 129–131.
- Pagliuso, P. G. *et al.* Evolution of the magnetic properties and magnetic structures along the $R_m\text{MIn}_{3m+2}$ ($R = \text{Ce, Nd, Gd, Tb}; M = \text{Rh, Ir}; m = 1, 2$) series of intermetallic compounds. *J. of App. Phys.* **99**, 08P703 (2006).
- Kubo, K. & Hotta, T. Orbital-Controlled Superconductivity in f -Electron Systems. *J. Phys. Soc. of Jpn.* **75** (2006) 083702.
- Bauer, E. *et al.* Structural Tuning of Unconventional Superconductivity in PuMGa_5 ($M = \text{Co, Rh}$). *Phys. Rev. Lett.* **93**, 147005 (2004).
- Sakakibara, H. *et al.* Multiorbital analysis of the effects of uniaxial and hydrostatic pressure on T_c in the single-layered cuprate superconductors. *Phys. Rev. B* **86**, 134520 (2012).
- Ohta, Y. *et al.* Apex oxygen and critical temperature in copper oxide superconductors: Universal correlation with the stability of local singlets. *Phys. Rev. B* **43**, 2968–2982 (1991).
- Granado, E. *et al.* Pressure and chemical substitution effects in the local atomic structure of BaFe_2As_2 . *Phys. Rev. B* **83**, 184508 (2011).
- Yin, Z. P., Haule, K. & Kotliar, G. Kinetic frustration and the nature of the magnetic and paramagnetic states in iron pnictides and iron chalcogenides. *Nature Materials* **10**, 932935 (2011).
- Abraham, A. & Bleaney, B. *EPR of Transition Ions* (Clarendon Press, Oxford, 1970).
- Poole, C. P. & Farach, H. A. *Relaxation in Magnetic Resonance*. (Academic Press, New York, 1971).
- Korringa, J. Nuclear magnetic relaxation and resonance line shift in metals. *Physica* **16**, 601 (1950).
- Davidov, D. *et al.* Electron spin resonance of Gd in the intermetallic compounds $\text{YCu, YAg, and LaAg}$: Wave vector dependence of the exchange interaction. *Solid State Comm.* **12**, 621 (1973).
- Hirst, L. L. Doubly Bottlenecked EPR in Cu: Cr, Mn. *Phys. Rev. B* **8**, 64–69 (1973).
- Hirst, L. L. Theory of the coupling between conduction electrons and moments of 3d and 4f ions in metals. *Advances in Physics* **27**, 231–285 (1978).



19. Narath, A. & Weaver, H. T. Effects of Electron-Electron Interactions on Nuclear Spin-Lattice Relaxation Rates and Knight Shifts in Alkali and Noble Metals. *Phys. Rev.* **175**, 373 (1968).
20. Shaw, R. W. & Warren, W. W. Enhancement of the Korringa Constant in Alkali Metals by Electron-Electron Interactions. *Phys. Rev. B* **3**, 1562 (1971).
21. Rettori, C. *et al.* Dynamic behavior of paramagnetic ions and conduction electrons in intermetallic compounds: $\text{Gd}_x\text{Lu}_{1-x}\text{Al}_2$. *Phys. Rev. B* **10**, 1826 (1974).
22. Pagliuso, P. G. *et al.* Electron spin resonance of Gd^{3+} and Nd^{3+} in LuInAs_4 ($A = \text{Cu}, \text{Ni}$). *Phys. Rev. B* **60**, 13515 (1999).
23. Urbano, R. R. *et al.* Multiband effects in the electron spin resonance of Gd^{3+} in the intermediate-valence compound YbAl_3 and its reference compound LuAl_3 . *Phys. Rev. B* **75**, 045107 (2007).
24. Bittar, E. M. *et al.* Probing the localized to itinerant behavior of the $4f$ electron in $\text{CeIn}_{3-x}\text{Sn}_x$ by Gd^{3+} electron spin. *Phys. Rev. B* **86**, 125108 (2012).
25. Yosida, K. Magnetic properties of Cu-Mn alloys. *Phys. Rev.* **106**, 893 (1957).
26. Rosa, P. F. S. *et al.* Evolution of Eu^{2+} spin dynamics in $\text{Ba}_{1-x}\text{Eu}_x\text{Fe}_2\text{As}_2$. *Phys. Rev. B* **86**, 165131 (2012).
27. Stewart, G. R. Superconductivity in Iron Compounds. *Rev. Mod. Phys.* **83**, 1589–1652 (2011) and references therein.
28. Dyson, F. J. Electron Spin Resonance Absorption in Metals. II. Theory of Electron Diffusion and the Skin Effect. *Phys. Rev.* **98** (1955), p. 349.
29. Wang, L. *et al.* Effects of Disordered Ru Substitution in BaFe_2As_2 : Possible Realization of Superdiffusion in Real Materials. *Phys. Rev. Lett.* **110**, 037001 (2013).
30. Moriya, T. The effect of electron-electron interaction on the nuclear spin relaxation in metals. *J. Phys. Soc. Jpn.* **18**, 516 (1963).
31. Narath, A. Nuclear Magnetic Resonance and Relaxation of ^{197}Au in Gold Metal and ^{109}Ag in Gold-Silver Alloys. *Phys. Rev.* **163**, 232 (1967).
32. Dengler, E. *et al.* Strong reduction of the Korringa relaxation in the spin-density wave regime of EuFe_2As_2 observed by electron spin resonance. *Phys. Rev. B* **81**, 024406 (2010).
33. Pascher, N. *et al.* Magnetic fluctuations and superconductivity in iron pnictides as probed by electron spin resonance. *Phys. Rev. B* **82**, 054525 (2010).
34. Ying, J. J. *et al.* Electron spin resonance in $\text{EuFe}_{2-x}\text{Co}_x\text{As}_2$ single crystals. *Phys. Rev. B* **81**, 052503 (2010).
35. Garitezi, T. M. *et al.* Synthesis and Characterization of BaFe_2As_2 Single Crystals Grown by In-flux Technique. *Braz. J. of Phys.* **43**, 223 (2013).
36. Thirupathaiah, S. PhD thesis. *Electronic structure studies of ferro-pnictide superconductors and their parent compounds using angle-resolved photoemission spectroscopy (ARPES)*. Berlin, 2011.
37. Lu, D. *et al.* Angle-Resolved Photoemission Studies of Quantum Materials. *Ann. Rev. of Cond. Matt. Phys.* **3**, 129–167 (2012).

Author contributions

P.F.S.R., C.A., T.M.G. and T. Grant grew the single crystals and performed pressure dependent transport measurements. P.F.S.R. performed ESR measurements. T.G. performed EDS measurements. P.F.S.R., C.A., T.M.G., T.G., Z.F., R.R.U., P.G.P. discussed the data and reviewed the manuscript.

Additional information

Competing financial interests: The authors declare no competing financial interests.

How to cite this article: Rosa, P.F.S. *et al.* Site specific spin dynamics in BaFe_2As_2 : tuning the ground state by orbital differentiation. *Sci. Rep.* **4**, 6543; DOI:10.1038/srep06543 (2014).



This work is licensed under a Creative Commons Attribution-NonCommercial-NoDerivs 4.0 International License. The images or other third party material in this article are included in the article's Creative Commons license, unless indicated otherwise in the credit line; if the material is not included under the Creative Commons license, users will need to obtain permission from the license holder in order to reproduce the material. To view a copy of this license, visit <http://creativecommons.org/licenses/by-nc-nd/4.0/>